ACS NANO

www.acsnano.org

ARTICLE

Ultrasound-Driven Two-Dimensional $Ti_3C_2T_x$ MXene Hydrogel Generator

Kang Hyuck Lee,[§] Yi-Zhou Zhang,[§] Qiu Jiang, Hyunho Kim, Abdulkader A. Alkenawi, and Husam N. Alshareef*

Cite This: *ACS Nano* 2020, 14, 3199–3207

Read Online

ACCESS | Metrics & More | Article Recommendations | Supporting Information

ABSTRACT: **Ultrasound is a source of ambient energy that is rarely exploited. In this work, a tissue-mimicking MXene-hydrogel (M-gel) implantable generator has been designed to convert ultrasound power into electric energy. Unlike the present harvesting methods for implantable ultrasound energy harvesters, our M-gel generator is based on an electroacoustic phenomenon known as the streaming vibration potential. Moreover, the output power of the M-gel generator can be improved by coupling with triboelectrification. We demonstrate the potential of this generator for powering implantable devices through quick charging of electric gadgets, buried beneath a centimeter thick piece of beef. The performance is attractive, especially given the extremely simple structure of the generator, consisting of nothing more than encapsulated M-gel. The generator can harvest energy from various ultrasound sources, from ultrasound tips in the lab to the probes used in hospitals and households for imaging and physiotherapy.**

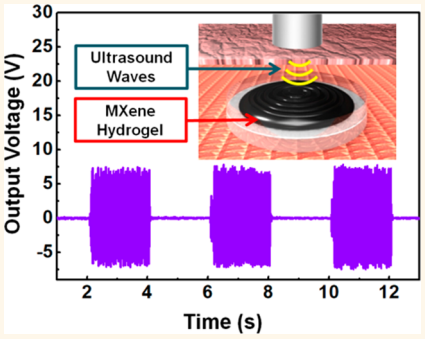

KEYWORDS: *ultrasound energy harvester, implantable device, wireless generator, hydrogel, MXene*

Ultrasound refers to sound waves with frequencies higher than the upper audible limit of human hearing, and it is widely utilized in many fields ranging from ultrasound imaging, object detection, and distance measurement represented by sonar, nondestructive testing, ultrasound cleaning, mixing, and accelerating chemical processes.[1−3] Among the various ambient energy sources, ultrasound is rarely exploited; however, it has great potential especially in the biomedical applications such as external charging of implantable devices through transferring its mechanical energy into electric power, as has been recently demonstrated by Hinchet *et al.*[4] They designed an ultrasound-driven triboelectric nanogenerator that can charge a lithium-ion battery at a charging rate of 166 μC/s even when buried beneath porcine tissues.

The major approaches to harvest ultrasound power are based on mechanisms such as piezoelectric[5,6] and triboelectric effects.[7−10] However, the present methods require specific materials and carefully designed complex device geometries to cause enough mechanical displacement of active materials to convert the acoustic energy into electric energy. Moreover, to make efficient implantable energy harvesters, biological tissue-mimicking materials with comparable bulk modulus and density to human tissues are needed to ensure biocompatibility and acoustic impedance matching.[11]

Hydrogels, a class of tissue-like semisolid ionic conductors, have attracted extensive interest as soft materials for flexible/stretchable electronics because of their advantages including superior flexibility, conformality to complex surfaces, tunable mechanical and electrical properties, multifunctionalities, and excellent biocompatibility.[12−14] It has recently been found that by developing composite hydrogels with reinforcing fillers, it is possible to increase the mechanical properties of hydrogels without sacrificing ionic conductivity[15−17] as well as to endow hydrogels with multifunctionalities such as magnetic[18,19] and luminescent[20−22] properties.

Transition-metal carbides, carbonitrides, and nitrides (MXenes) are a new family of two-dimensional (2D) nanomaterials, with the general formula of $M_{n+1}X_nT_x$ (M, X, T_x represent an early transition metal, carbon, and/or nitrogen, surface terminations such as hydroxyl, oxygen, or fluorine, respectively). The typical $Ti_3C_2T_x$ MXene possesses a 2D lamellar structure, hydrophilic surface properties, high electric conductivity, and the ability to host many different cations between their layers.[23−26] These exceptional properties have attracted wide research attention from various fields such as energy storage, catalysis, and sensing.[27−32] The combination of $Ti_3C_2T_x$ MXene with organic molecules or polymers exhibits

Received: October 25, 2019
Accepted: February 20, 2020
Published: February 20, 2020

https://dx.doi.org/10.1021/acsnano.9b08462
ACS Nano 2020, 14, 3199–3207

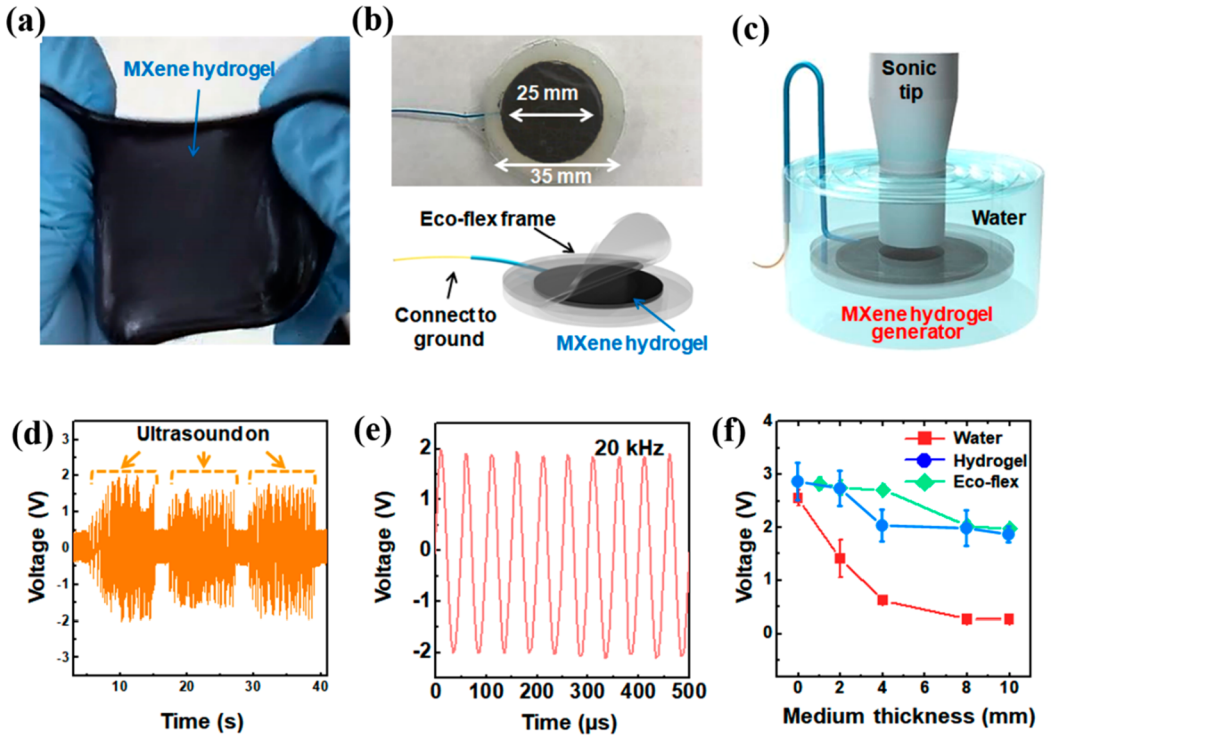

Figure 1. Electric power generation by ultrasound propagation in MXene hydrogel (M-gel). (a) Photo of the stretchable M-gel. (b) Photo of the M-gel generator and its schematic illustration. (c) Schematic showing the testing setup used to study the M-gel generator. (d) Generated voltage of the M-gel generator at 10 MΩ load resistance. (e) The voltage waveform produced by the M-gel generator, which is measured by an oscilloscope at the microsecond time scale. (f) Output voltages of the M-gel generators in water, eco-flex, and hydrogel mediums, as a function of medium thickness.

synergistic properties such as high electrical, chemical, electrochemical performances, superior mechanical properties, and biocompatibility since molecules or polymers can be aligned on the oxygen- or fluorine-terminated surface of $Ti_3C_2T_x$ layers through hydrogen bonding.[33−36]

Recently we have demonstrated that MXenes and poly(vinyl alcohol) (PVA) can form a three-dimensional (3D) network-structured hydrogel.[37] The obtained MXene-based hydrogel (M-gel) shows not only largely increased mechanical properties, but more importantly an asymmetrical strain sensitivity. The interesting properties of M-gel can be attributed to the synergistic effect arising from the bonding between the 2D structured MXenes with negatively charged surfaces and PVA chains.[37] Given the vast potential of hydrogels in various fields, it is anticipated that novel devices with unexpected electrochemical and electromechanical properties can be built based on the M-gel.

In this work, we demonstrate that the M-gel can generate sufficient electric power from ultrasound to power electric gadgets. Instead of the common piezoelectric or triboelectric effects, we attribute the energy harvesting ability of M-gel to the streaming vibration potential (SVP) which describes the coupling between acoustic and electric fields when ultrasound propagates through a fluid-containing capillary, microchanneled, and porous body.[38−41] Moreover, the output power of the generator can be improved by coupling with triboelectrification. The M-gel generator has demonstrated utility in applications such as quick charging of a capacitor and as the power source for an electric hygrometer. The vast application potential of our generator is demonstrated by harvesting power from ultrasound beneath the skin (demonstrated by using a piece of beef with centimeter thickness) and by using various ultrasound sources from those used in the lab to those used in hospitals and households.

RESULTS AND DISCUSSION

Titanium carbide MXene ($Ti_3C_2T_x$) nanosheets were prepared through etching and delamination of a MAX (Ti_3AlC_2) precursor following a previous report,[37] with an obtained MXene nanosheet size ranging from 1 to 5 μm (Figure S1a). The high quality of the obtained MXene nanosheets was demonstrated by high-resolution transmission electron microscopy (HRTEM, Raman spectroscopy, and X-ray diffraction (XRD) (Figure S1). The obtained MXene nanosheets were mixed with a commercial PVA-hydrogel "crystal clay" which contains PVA, water, and antidehydration additives, resulting in a stretchable MXene PVA-hydrogel composite (M-gel) (Figure 1a).

The structure of the M-gel generator can be described as follows: A uniform layer of M-gel with a thickness of 1 mm was sandwiched between two flexible eco-flex frames and connected to the grounded probe of an oscilloscope (the internal impedance of the probe was 10 MΩ) through a coated copper wire, as shown in Figure 1b. The eco-flex frames were used to confine the M-gel into fixed shapes as well as to prevent the M-gel from swelling in water. Ultrasound waves were propagated to the M-gel generator across a water medium with 2 mm thickness from a tip-sonicator, as shown in Figure 1c. The frequency and power density of the ultrasound wave were 20 kHz and 0.1W/cm^2, respectively. The ultrasound wave was turned on at constant intervals to clearly distinguish the on/off states. Importantly, we discovered that the M-gel

https://dx.doi.org/10.1021/acsnano.9b08462
ACS Nano 2020, 14, 3199−3207

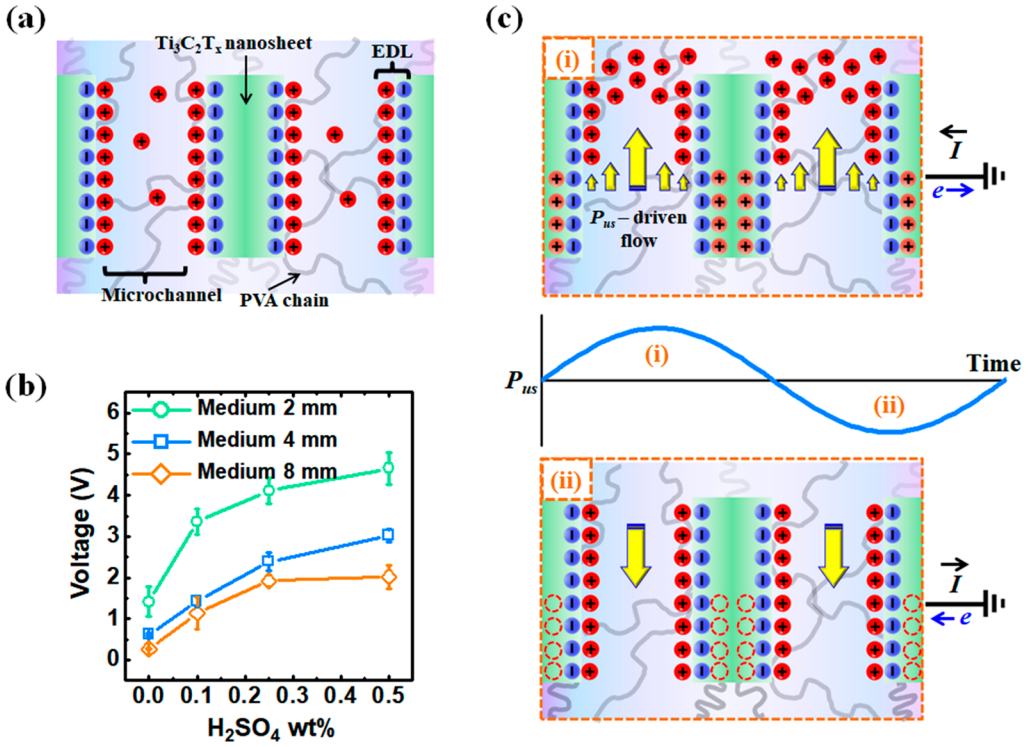

Figure 2. The proposed mechanism for voltage generation phenomenon in the M-gel generators. (a) Schematic showing the formation of the EDL within the $Ti_3C_2T_x$ MXene-PVA hydrogel. (b) Output voltage profile of the M-gel generators as a function of H_2SO_4 wt % in the M-gel using eco-flex medium of various thicknesses. (c) Schematic illustration of the proposed electrical signal generation mechanism of M-gel driven by the propagation of the ultrasound wave.

generator could produce electric power with alternating voltage (Figure 1d) profiles as the ultrasound waves propagate through the M-gel. The output voltage was ∼2 V. In contrast, the pristine PVA-hydrogel without MXene nanosheets only generated very low voltage under the same ultrasound wave condition (Figure S2) used for the M-gel device, which reveals the key role that MXene nanosheets play in the power generation behavior of the M-gel generator. Interestingly, the output voltage of the M-gel generator exhibited a clear sine waveform with a frequency of 20 kHz, which perfectly matches the ultrasound waveform input into the device (Figure 1e).

In the M-gel generator (Figure 1c), ultrasound waves have to travel through interfaces between both water/eco-flex and eco-flex/M-gel. The ultrasound energy is lost partly due to reflection at interfaces characterized by the acoustic impedance mismatching of media;[42] partly due to absorption in the medium which causes a continuous attenuation of energy.[42,43] To figure out how the reflectance and absorption within media affect the device performance, we measured the output voltages of the M-gel generators with water, eco-flex, PVA-hydrogel, and air media, respectively. The initial output voltages with the water, eco-flex, and hydrogel media were almost the same at around 2.8 V (at the initial stage, the sonic-tip is in direct contact with the top eco-flex layer of the M-gel generator, and we define it as "zero thickness of medium" in the graphs). The output voltage was reduced to 0.37, 2.14, and 1.89 V when the thickness of water, eco-flex, and hydrogel medium were each increased to 10 mm, as shown in Figure 1f. This is because the acoustic attenuation in homogeneous medium is proportional to the frequency and travel distance (*i.e.*, the thickness of the medium) of ultrasound waves.[42,43] Although water has a much smaller acoustic attenuation coefficient compared to eco-flex,[43] the voltage of M-gel generator with 10 mm thickness of eco-flex medium is 5 times higher than that with the same thickness of water. The reflection coefficient between the inserted eco-flex layer as the medium and the eco-flex top layer of the M-gel generator is zero since these are the same media. This reveals that the output performance of M-gel generator is predominantly affected by presence of reflectance. Moreover, the similarity of the voltage reduction behavior of the M-gel generator with eco-flex and hydrogel media implies that there is low reflectance between the hydrogel and eco-flex encapsulation layer. To clarify the internal voltage reduction effect caused by the eco-flex encapsulation layer in the M-gel generator, we measured the output voltage of M-gel generators with and without the eco-flex encapsulation layer under the ultrasound wave and confirmed that the reduction in the output voltage caused by eco-flex layer was only 8.4% (Figure S3). This observation suggests that the loss in ultrasound energy is minimized in the M-gel generator and the possibility of using the M-gel generator to effectively convert ultrasound energy into electrical energy in the presence of a thick medium (Figure 1f, Movie S1). Furthermore, the acoustic reflectance coefficient is calculated to be low (4.4−6.0%) based on the acoustic impedance of eco-flex (∼1.03 MRayl) and human tissues (1.58−1.70 MRayl).[11,42,44] The above results show the great potential of the M-gel generator for powering implantable devices.

As we found in our previous work,[37] $Ti_3C_2T_x$ nanosheets can form a 3D network structure in the PVA-hydrogel matrix which contains a large amount of water. In other words, the M-gel can be considered a kind of porous body filled with water as shown in Figure 2a. It is well-known that a pressure-driven

https://dx.doi.org/10.1021/acsnano.9b08462
ACS Nano 2020, 14, 3199−3207

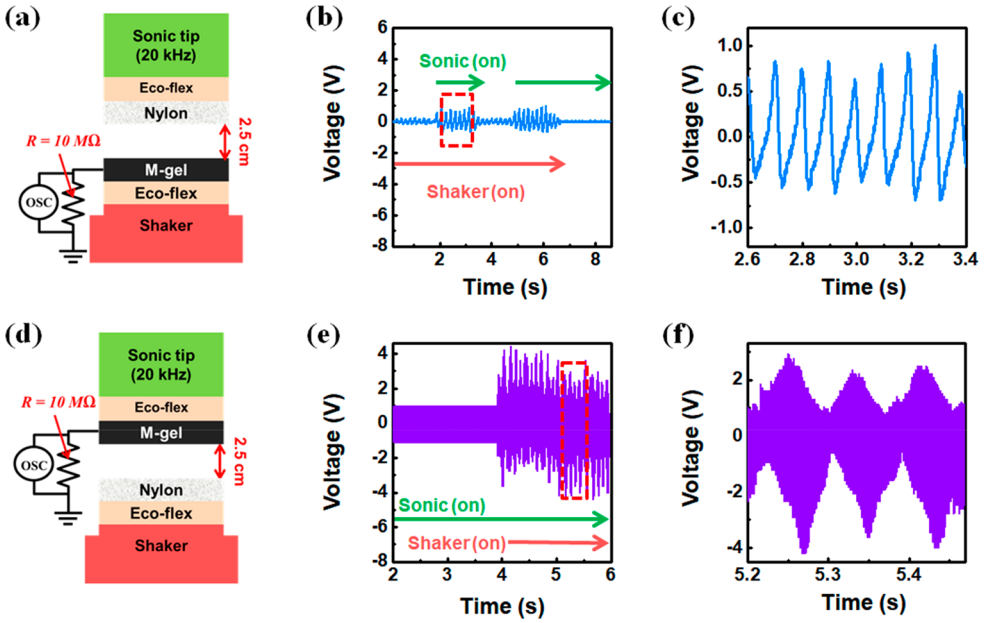

Figure 3. Model experiments used to investigate the influence of triboelectrification. (a) Schematic of experimental set up, where ultrasound waves are applied to the Ny/eco-flex stack, and the shaker vibrates at 10 Hz on the M-gel. (b) The output voltages for the experiment shown in (a) and (c) magnification of the "sonic on" region shown in (b). (d) Schematic of experimental set up, where ultrasound waves are applied to M-gel layer and shaker makes vibration on the eco-flex/nylon stacking. (e) The output voltages of experiment shown in (d) and (f) magnification of the "shaker on" region shown in (e).

flow can drag excess counterions inside the electrical double layer (EDL) to move near a charged surface, generating an electric current termed streaming current. In the absence of an external electrical load, a streaming potential is developed to balance the streaming current,[43,45] and in the cases where pressure is generated by ultrasound, it is called SVP. Generally, the SVP generation has been found in microchannel,[46,47] fiber,[48,49] and porous film.[50,51] Recently, it was also found in composite hydrogels.[41,52,53] Thus, the power generation behavior of the M-gel generator can be attributed to the SVP.

If the voltage generation behavior of the M-gel was indeed caused by the oscillation of charges in the EDL, as the SVP theory predicts, the output voltage should be affected by the ionic state within the hydrogel. This is because $Ti_3C_2T_x$ MXene has a high volumetric capacitance in acid electrolytes such as H_2SO_4,[27,54] leading to a higher density of charges in the EDL of the MXene nanosheet network. To confirm this, we measured the ultrasound-driven output voltage of M-gel generators having different eco-flex medium thickness and different wt % of H_2SO_4. It turns out that the power generation performance can indeed be improved by changing the electrolytic state of the M-gel; in fact, as we added 0.1−0.5 wt % of H_2SO_4 into the M-gel, the output voltage almost tripled, regardless of the thickness of eco-flex medium (Figure 2b, Figure S4). The ultrasound energy harvesting mechanism of the M-gel generator is schematically illustrated in Figure 2c. When ultrasound waves propagate through the MXene nanosheet network, the pressure-driven water flow can be generated, which would drag out counterions of the EDL on the surface of MXene nanosheets as it passes through the interfaces within the network structure. This effect causes a potential difference between the exposed negatively charged surfaces and the accumulated cations within the flow, in the direction of the ultrasound propagation. This potential can induce extra electrons to move toward the external ground electrode away from the MXene nanosheets (Figure 2c, up). As the ultrasound waves progress further, the compressed cation layer relaxes and electrons flow from the ground electrode back into the MXene layers to achieve electrostatic balance (Figure 2c, down). As a result, AC signals are generated due to the oscillation in the number of cations in the EDL of the MXene network, driven by the pressure gradient caused by the ultrasound wave.

We designed two model experiments to investigate whether mechanical friction contributes to power generation in our device. This is because we cannot completely exclude the effect of triboelectrification in the M-gel generator as might be caused by the ultrasound waves. The first experiment (Figure 3a) was designed to figure out whether the ultrasound source used for the power generation of M-gel generator can induce triboelectrification between physically contacted tribo-pair (eco-flex and nylon), and how the M-gel electrode responds to this tribo-pair. We attached the grounded M-gel electrode on an eco-flex substrate which was placed on a shaker and fixed an eco-flex/nylon layer with identical size to the bottom of a sonic tip hanging on top of the M-gel. The two surfaces were separated with a 2.5 cm spacing to prevent physical contact between the nylon and M-gel surfaces (the minimum distance between M-gel and nylon surfaces that can be approached by the shaker was 10 mm). The oscillation of the M-gel caused by the shaker (10 Hz) produced a small AC voltage of around 0.2 V, which increased dramatically upon applying ultrasound waves to the eco-flex/nylon layer (Figure 3b). The small voltage generated by the movement of the shaker can be attributed to the electrostatic induction caused by the positive-charged surface of nylon approaching/moving away from a grounded conductor (M-gel).[55] Generally, nylon tends to give up electrons when brought in contact with other materials,[56] therefore, nylon in the eco-flex/nylon layer would become positively charged being in contact with eco-flex. The applied

https://dx.doi.org/10.1021/acsnano.9b08462
ACS Nano 2020, 14, 3199−3207

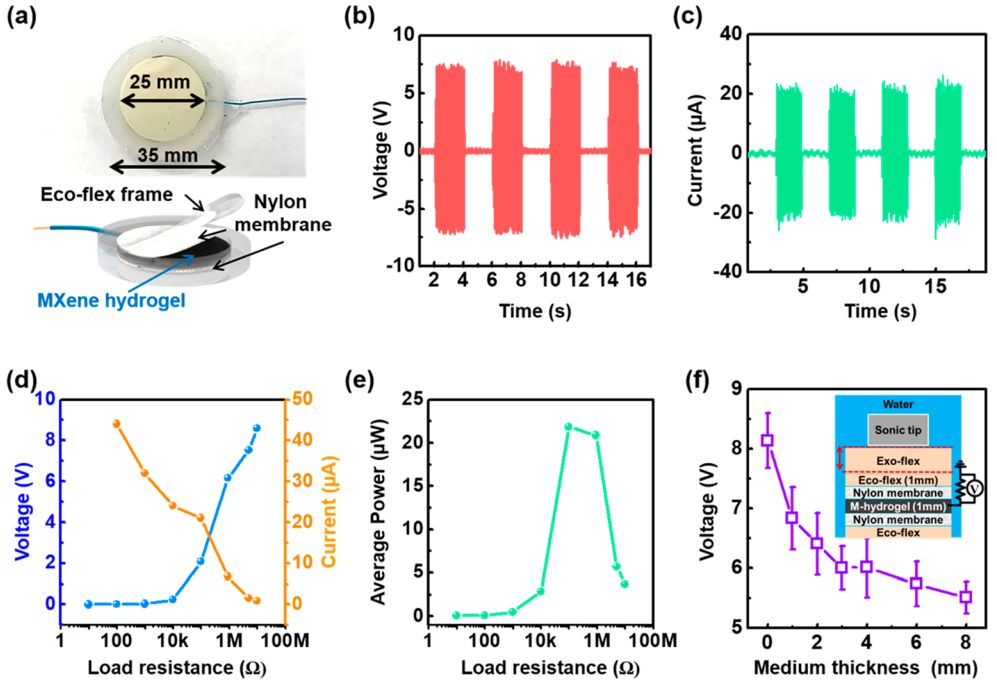

Figure 4. Output performance of the enhanced M-gel generator. (a) Image of the enhanced M-gel generator and its schematic illustration. (b) Voltage output with 10 MΩ load resistance, and (c) current output with 100 kΩ load resistance under 20 kHz of ultrasound wave. (d) The output voltage and output current as a function of load resistance. (e) The power output as a function of load resistance. (f) The output voltage measured as a function of the eco-flex medium thickness.

ultrasound waves would induce a friction between nylon and eco-flex, and positive charges would build up. Thus, the larger voltage upon applying ultrasound is due to the friction between eco-flex and nylon layers caused by ultrasound waves. However, as shown in Figure 3c, the frequency of the generated voltage is the same as the frequency of the shaker (10 Hz), even when applying ultrasound. This means that applying ultrasound waves to the eco-flex/nylon layer cannot make voltage signals out of the M-gel without oscillation of shaker. This experiment shows that although ultrasound waves can generate sufficient frictional charges on the nylon layer, it cannot cause enough mechanical displacement to induce potential difference in the M-gel.

To better clarify this issue, we prepared eco-flex, aluminum (Al), and MXene films and measured their voltage output performance in the single-electrode triboelectric generator (STEG) geometry through pushing tests, as shown in Figure S5a,b. The triboelectric induced voltage of the eco-flex/MXene film was much lower than the eco-flex/Al film (Figure S5c). It means that triboelectric effect between eco-flex and MXene film is much lower than between eco-flex and Al. If the ultrasound-driven voltage generation of the M-gel generator was originated from the triboelectric phenomenon, the eco-flex/Al film device would have shown higher voltage than the M-gel generator under ultrasound waves. However, when the M-gel in the M-gel generator was replaced with an Al film, it shows a lower voltage with irregular waveform (Figure S6). From the above results, it is hard to explain the conversion of ultrasound power by the common triboelectrification phenomena.

The second model experiment was designed to investigate how fluctuations of external electric fields can influence the voltage generation behavior of the M-gel generator. Thus, in contrast to the first experiment (Figure 3a), we applied ultrasonic waves to M-gel and measured the output voltage when the charged eco-flex/nylon layer (the nylon layer was precharged by rubbing with PI film) was oscillated by the shaker, as shown in Figure 3d. When applying ultrasound waves to the M-gel, an AC signal of 1 V appeared with the same frequency as the ultrasound; however, the voltage rapidly increased due to the repetitive approaching of the charged nylon surface (Figure 3e). Interestingly, unlike in the first model experiment (Figure 3c), the output voltage has the same frequency as the incoming ultrasound waves, and its amplification period coincides with the frequency of the shaker as shown in Figure 3f.

The results from these two model experiments indicate two important facts: First, in the M-gel generator, ultrasound waves can cause triboelectrification which makes significant electrostatic induction in the presence of a triboelectric pair. Second, the voltage generated by the M-gel generator under ultrasound waves can be increased under external electrostatic fields.

The above findings indicate a potential approach to enhance the power generation performance of the M-gel device under ultrasounds, which is by coupling with triboelectric charge induction. To test this hypothesis, a layer of porous nylon was placed between the M-gel and the eco-flex encapsulation layers (Figure 4a). Interestingly, a four times improvement was observed in the output voltage reaching ~8 V at the load resistance of 10 MΩ (Figure 4b and Movie S2) for the triboelectrically enhanced generator as compared to the pristine one, and a current of 21 μA was generated at the load resistance of 100 kΩ (Figure 4c). The output voltage has the same frequency as the incoming ultrasound waves (Movie S3). To determine the optimal load resistance, we measured the output voltage and current of the enhanced M-gel generator as a function of load resistances (Figure 4d) and summarized the calculated average powers in Figure 4e. The

https://dx.doi.org/10.1021/acsnano.9b08462
ACS Nano 2020, 14, 3199−3207

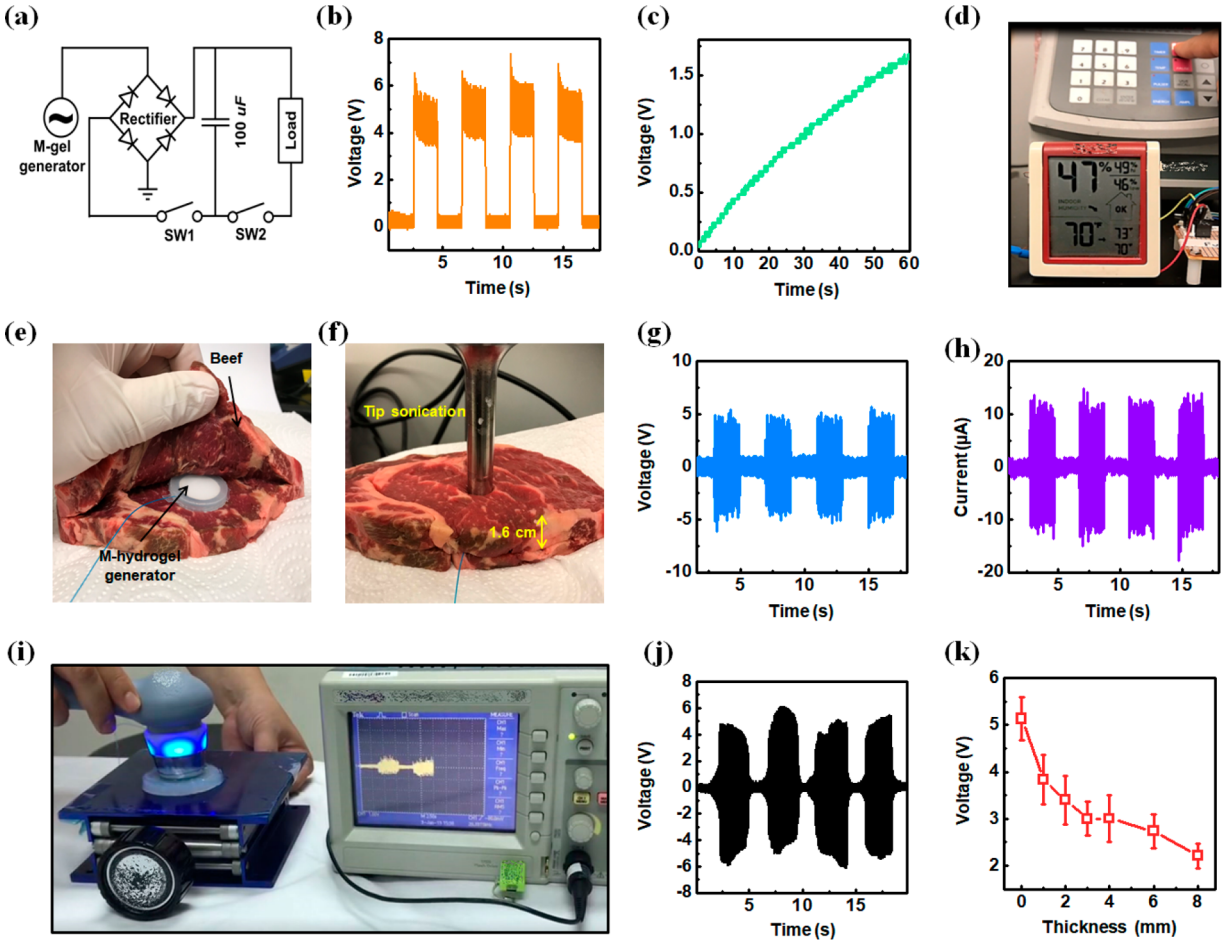

Figure 5. Applications of the M-gel generator. (a) Circuit diagram of the M-gel generator for practical applications. (b) Rectified voltage output of the M-gel generator. (c) Charging curve of the capacitor (100 uF) connected to the circuit. (d) Photograph of the electric hygrometer powered by the M-gel generator. (e) Encapsulation of the M-gel generator inside a piece of beef and (f) measurement setup. (g) Voltage and (h) current generated by the M-gel generator inside a piece of beef. Load resistances of 10 MΩ and 100 kΩ were used for the voltage and current measurements, respectively. (i) Photo showing ultrasound energy harvesting behavior of the M-gel generator using a medical ultrasound probe for physiotherapy. (j) Corresponding normalized voltage output of the M-gel generator using medical ultrasound probe. (k) Ultrasound-induced voltage output measured as a function of medium thickness between the ultrasound tip and the generator.

enhanced M-gel generator was able to generate an average power of 21.8 μW at the optimized load resistance of 100 kΩ from the incident ultrasound power of 0.1 W/cm^2. If using the ultrasound beam incident area as the effective area of the generator, the power conversion efficiency of enhanced M-gel generator is calculated to be 0.021%. It is comparable with the efficiency of the triboelectric implantable ultrasound harvester reported very recently to show outstanding performance.[4] The output voltage of the enhanced M-gel generator can be maintained at above 5 V, even with a thick medium (Figure 4f). With these output performances, the triboelectrically enhanced M-gel generator has huge application potentials.

To show the potential of the enhanced M-gel generator with its high output power and high conversation efficiency as a sustainable and clean power source, some practical applications have been demonstrated with the circuit diagram shown in Figure 5a. The generator produced a rectified voltage of above 6 V (Figure 5b). When a capacitor (100 uF) was connected to the circuit, the voltage of the capacitor increased to 1.68 V in 60 s (Figure 5c), resulting in an average charging rate of 2.8 μC/s. The electrical power of the enhanced M-gel generator is sufficient to continuously drive common electric gadgets such as an electric hygrometer (Figure 5d, Movies S4 and S5). To test the feasibility of the generator for *in vivo* applications, we inserted the enhanced M-gel generator within a piece of fresh beef with a thickness relevant for implantable devices (Figure 5e,f, Movie S6). The output signals of enhanced M-gel generator were ~4.5 V and 14.4 μA at the load resistance of 10 MΩ and 100 kΩ, respectively (Figure 5g,h). The voltage of the enhanced M-gel generator buried within the beef tissue (16 mm) was only 5.5% lower than the output voltage under 8 mm thickness of eco-flex (Figure 4f) due to the small acoustic impedance mismatching between eco-flex and the beef tissues.[11,57,58] Apart from ultrasound tips used in the lab, the generator can also harvest ultrasound energy from common medical ultrasound probes for both imaging (ESAOTE, MyLabTM ClassC) (Movie S7) and physical therapy (BTL, BTL−4710) (Figure 5i and Movie S8). In the case of using the imaging probe, a ~5 V voltage output can be observed (Figure 5j), which remains above 2 V even with an eco-flex medium of 8 mm thickness.

CONCLUSION

In summary, we have developed a facile method to convert ultrasound power into electric energy using a $Ti_3C_2T_x$ MXene-PVA hydrogel. The M-gel can produce a special electroacoustic

https://dx.doi.org/10.1021/acsnano.9b08462
ACS Nano 2020, 14, 3199−3207

phenomenon known as the streaming vibration current/potential, which leads to high output electric power when ultrasound waves pass through the M-gel containing device. The potential of this generator is demonstrated through the quick charging of electric gadgets, even when buried within a piece of beef with centimeter thickness. This performance is attractive, especially given the extremely simple structure of the generator, consisting of nothing more than encapsulated M-gel. This is unlike the other methods used to harvest ultrasound energy which require specific materials and carefully designed complex device geometry. The huge potential of the generator is also demonstrated by using different ultrasound sources, ranging from ultrasound tips in the lab to various ultrasound probes used in hospitals and households for both imaging and physiotherapy.

METHODS

Synthesis of MXene Nanosheets and M-gel. $Ti_3C_2T_x$ MXene was synthesized following the LiF/HCl method.[37] The etching solution was prepared by adding 1.5 g of LiF to 10 mL of 6 M hydrochloric acid followed by stirring for 5 min. Then, 2 g of Ti_3AlC_2 powder was slowly added to the etchant at 35 °C and stirred for 24 h. The acidic suspension was washed with deionized (DI) water until a pH of 6 was reached *via* centrifugation at 3500 rpm (5 min per cycle) and decanting of the supernatant after each cycle. The MXene nanosheets were collected *via* centrifugation at 3500 rpm for 5 min.

The MXene-based hydrogel (M-gel) was prepared in the following way: First, MXene paste was obtained from collecting the sediment after centrifugation of the MXene suspension at 8000 rpm for 60 min. The water content in the MXene paste was around 96.7−98% and was calculated from the weight difference between MXene paste and its dehydrated state. Then, the MXene paste was spread on pristine hydrogel, and the mixed hydrogel was rolled into a ball and flattened by hand. This process was repeated 3−5 times until the color of the mixture became uniformly black, as shown in Figure 1a. This rolling and flattening process was conducted at room temperature (25 °C) and relative humidity of about 55% RH. We used commercially obtained PVA-hydrogel (Genius boys, Liaocheng wisdom and fun, Co. Ltd., Crystal-clay, China) to prepare the M-gel. The PVA-hydrogel was left in air for about 10 min including the mixing process before putting it in the device. The weight loss of the PVA-hydrogel due to the dehydration was negligible at this time scale. The weight percentages of M-gels were determined as the dried weight of MXenes divided by the total weight of the corresponding M-gel.

Synthesis of H_2SO_4-containing M-gel. Dilute H_2SO_4 aqueous solutions were added dropwise to the M-gel until the weight percentages of 0.1%, 0.25%, and 0.5% were obtained.

Output Voltage and Current Measurement of the M-gel Generators. To measure the output voltage of the M-gel generators, we connected M-gel to an electrical probe which has an internal impedance of 10 MΩ, with its other side grounded, and measured the output voltage by an oscilloscope (Tektronix, TDS 2024B) under the application of ultrasound waves. The ultrasound waves were generated by tip-sonicator (Sonic & Materials Inc., UP-VC750, diameter of the tip is 13 mm) with a power amplitude of 50%. The output currents of the M-gel generator were measured by Keithly 6514 electrometer with certain load resistances (1 Ω to 10 MΩ). The intensity of ultrasound waves was measured using an ultrasonic power meter (Ultrasonic Equipment, YP0511A, China) in water.

To test ultrasound energy harvesting performances of the M-gel generator from common medical ultrasound sources, a liner probe for the ultrasound imaging system (ESAOTE, MyLab ClassC,) and a round probe of ultrasound therapy system (BTL, BTL−4710) were used. The frequencies of ultrasonic waves generated from imaging and therapy probes were 12 and 3 MHz, respectively. The output voltage was measured after applying the ultrasonic gel to the surface of the M-gel generator to minimize the loss of ultrasonic energy and the friction effect. Different thicknesses of the eco-flex layers (1, 2, 3, 4, 6, and 8 mm) were used as media between probe and top layer of the M-gel generator to investigate the medium thickness effect.

ASSOCIATED CONTENT

Supporting Information

The Supporting Information is available free of charge at https://pubs.acs.org/doi/10.1021/acsnano.9b08462.

Characterization of $Ti_3C_2T_x$ MXene nanosheets; ultrasound-driven voltage generation of PVA-hydrogel generator; output voltage reduction of the M-gel generator by the eco-flex encapsulation layer; increase of the output voltage of M-gel generator upon addition of H_2SO_4; triboelectric voltage induction of thin films by the pushing test; voltage induction of eco-flex encapsulated Al-foil by ultrasound waves; electrostatic induction between Al and nylon/eco-flex by the ultrasound waves; voltage generation of the M-hydrogel generator using medical ultrasound probe; ultrasound-driven voltage generation of graphene-hydrogel generator (PDF)

Movie S1. Ultrasound-driven electrical power generation of the M-gel generator with 8 mm eco-flex medium (AVI)

Movie S2. Ultrasound-driven electrical power generation of the enhanced M-gel generator (AVI)

Movie S3. The enhanced M-gel generator shows high frequency voltage signal with the same frequency as the applied ultrasound waves (AVI)

Movie S4. Electronic hygrometer powered by a capacitor precharged by the enhanced M-gel generator for 60 s (AVI)

Movie S5. Electronic hygrometer powered by the enhanced M-gel generator (AVI)

Movie S6. Performances of the enhanced M-gel generator with beef medium (AVI)

Movie S7. Voltage generation of the enhanced M-gel generator by an ultrasound imaging probe (12 MHz) (AVI)

Movie S8. Voltage generation of the enhanced M-gel generator by an ultrasound probe for physiotherapy (3 MHz) (AVI)

Movie S9. Voltage generation of the enhanced M-gel generator with 8 mm eco-flex medium by an ultrasound probe for physiotherapy (3 MHz) (AVI)

AUTHOR INFORMATION

Corresponding Author

Husam N. Alshareef − *Materials Science and Engineering, Physical Science and Engineering Division, King Abdullah University of Science and Technology (KAUST), Thuwal 23955-6900, Saudi Arabia;* orcid.org/0000-0001-5029-2142; Email: husam.alshareef@kaust.edu.sa

Authors

Kang Hyuck Lee − *Materials Science and Engineering, Physical Science and Engineering Division, King Abdullah University of Science and Technology (KAUST), Thuwal 23955-6900, Saudi Arabia*

Yi-Zhou Zhang − *Materials Science and Engineering, Physical Science and Engineering Division, King Abdullah University of Science and Technology (KAUST), Thuwal 23955-6900, Saudi Arabia*

https://dx.doi.org/10.1021/acsnano.9b08462
ACS Nano 2020, 14, 3199−3207

Qiu Jiang − *Materials Science and Engineering, Physical Science and Engineering Division, King Abdullah University of Science and Technology (KAUST), Thuwal 23955-6900, Saudi Arabia*

Hyunho Kim − *Materials Science and Engineering, Physical Science and Engineering Division, King Abdullah University of Science and Technology (KAUST), Thuwal 23955-6900, Saudi Arabia;* orcid.org/0000-0003-2381-9716

Abdulkader A. Alkenawi − *College of Applied Medical Science, King Saud bin Abdulaziz University for Health Sciences, Jeddah 22384, Saudi Arabia*

Complete contact information is available at: https://pubs.acs.org/10.1021/acsnano.9b08462

Author Contributions

[§]These authors contributed equally. K.H.L. and Y.-Z.Z. designed and conceptualized the project, designed the experiments, and analyzed the data. Q.J. and H.K. synthesized and characterized the $Ti_3C_2T_x$ MXenes. A.A.A. provided guidance on experiments using medical ultrasound systems. H.N.A. supervised the overall conception and design of this project. All authors contributed to the writing of the paper and gave approval to the final version.

Notes

The authors declare no competing financial interest.

ACKNOWLEDGMENTS

Research reported in this publication is supported by King Abdullah University of Science and Technology (KAUST). The authors thank Professor Khaled Salama and Professor Zhong Lin Wang for several useful comments.

REFERENCES

(1) Wang, L. V.; Hu, S. Photoacoustic Tomography: *In Vivo* Imaging from Organelles to Organs. *Science* **2012**, *335*, 1458−1462.

(2) Lamminen, M. O.; Walker, H. W.; Weavers, L. K. Mechanisms and Factors Influencing the Ultrasonic Cleaning of Particle-Fouled Ceramic Membranes. *J. Membr. Sci.* **2004**, *237*, 213−223.

(3) Bang, J. H.; Suslick, K. S. Applications of Ultrasound to the Synthesis of Nanostructured Materials. *Adv. Mater.* **2010**, *22*, 1039−1059.

(4) Hinchet, R.; Yoon, H. J.; Ryu, H.; Kim, M. K.; Choi, E. K.; Kim, D. S.; Kim, S. W. Transcutaneous Ultrasound Energy Harvesting Using Capacitive Triboelectric Technology. *Science* **2019**, *365*, 491−494.

(5) Park, K. I.; Xu, S.; Liu, Y.; Hwang, G. T.; Kang, S. J. L.; Wang, Z. L.; Lee, K. J. Piezoelectric $BaTiO_3$ Thin Film Nanogenerator on Plastic Substrates. *Nano Lett.* **2010**, *10*, 4939−4943.

(6) Zhang, G.; Zhao, P.; Zhang, X.; Han, K.; Zhao, T.; Zhang, Y.; Jeong, C. K.; Jiang, S.; Zhang, S.; Wang, Q. Flexible Three-Dimensional Interconnected Piezoelectric Ceramic Foam Based Composites for Highly Efficient Concurrent Mechanical and Thermal Energy Harvesting. *Energy Environ. Sci.* **2018**, *11*, 2046−2056.

(7) Yang, J.; Chen, J.; Liu, Y.; Yang, W.; Su, Y.; Wang, Z. L. Triboelectrification-Based Organic Film Nanogenerator for Acoustic Energy Harvesting and Self-Powered Active Acoustic Sensing. *ACS Nano* **2014**, *8*, 2649−2657.

(8) Fan, X.; Chen, J.; Yang, J.; Bai, P.; Li, Z. L.; Wang, Z. L. Ultrathin, Rollable, Paper-Based Triboelectric Nanogenerator for Acoustic Energy-Harvesting and Self-Powered Sound Recording. *ACS Nano* **2015**, *9*, 4236−4243.

(9) Yu, A. F.; Song, M.; Zhang, Y.; Zhang, Y.; Chen, L. B.; Zhai, J. Y.; Wang, Z. L. Self-Powered Acoustic Source Locator in Underwater Environment Based on Organic Film Triboelectric Nanogenerator. *Nano Res.* **2015**, *8*, 765−773.

(10) Xi, Y.; Wang, J.; Zi, Y.; Li, X.; Han, C.; Cao, X.; Hu, C.; Wang, Z. High Efficient Harvesting of Underwater Ultrasonic Wave Energy by Triboelectric Nanogenerator. *Nano Energy* **2017**, *38*, 101−108.

(11) Hu, Y. C.; Liao, P. L.; Shih, W. P.; Wang, X. Y.; Chang, P. Z. Study on the Acoustic Impedance Matching of Human Tissue for Power Transmitting/ Charging System of Implanted Biochip. Proceedings from the *2009 IEEE 3rd International Conference on Nano/Molecular Medicine and Engineering (NANOMED)*, October 18−21, 2009; IEEE: Piscataway, NJ, 2009.

(12) Yang, C.; Suo, Z. Hydrogel Ionotronics. *Nat. Rev. Mater.* **2018**, *3*, 125−142.

(13) Calvert, P. Hydrogel for Soft Machines. *Adv. Mater.* **2009**, *21*, 743−756.

(14) Keplinger, C.; Sun, J.-Y.; Foo, C. C.; Rothemund, P.; Whitesides, G. M.; Suo, Z. Stretchable, Transparent, Ionic Conductors. *Science* **2013**, *341*, 984−987.

(15) Min, J. H.; Patel, M.; Koh, W.-G. Incorporation of Conductive Materials into Hydrogels for Tissue Engineering Applications. *Polymers* **2018**, *10*, 1078.

(16) Cha, C.; Shin, S. R.; Gao, X.; Annabi, N.; Dokmeci, M. R.; Tang, X. S.; Khademhosseini, A. Controlling Mechanical Properties of Cell-Laden Hydrogels by Covalent Incorporation of Graphene Oxide. *Small* **2014**, *10*, 514−523.

(17) Ge, G.; Zhang, Y. Z.; Shao, J. J.; Wang, W. J.; Si, W. Li.; Huang, W.; Dong, X. C. Stretchable, Transparent, and Self-Patterned Hydrogel-Based Pressure Sensor for Human Motions Detection. *Adv. Funct. Mater.* **2018**, *28*, 1802576.

(18) Weeber, R.; Kantorovich, S.; Holm, C. Ferrogels Cross-Linked by Magnetic Particles: Field-Driven Deformation and Elasticity Studied Using Computer Simulations. *J. Chem. Phys.* **2015**, *143*, 154901.

(19) Gonzalez, J. S.; Hoppe, C. E.; Muraca, D.; Sánchez, F. H.; Alvarez, V. A. Synthesis and Characterization of PVA Ferrogels Obtained-through a One-Pot Freezing-Thawing Procedure. *Colloid Polym. Sci.* **2011**, *289*, 1839−1846.

(20) Ostakhov, S. S.; Kayumova, R. R.; Vildanova, R. R.; Sigaeva, N. N.; Khusnitdinov, I. I.; Kolesov, S. V.; Khursan, S. L. Spectral-Luminescent Study of a Hydrogel Based on Hyaluronic Acid Dialdehyde and Chitosan Succinate Containing the Lucentis Drug. *High Energy Chem.* **2018**, *52*, 34−37.

(21) Xia, Y.; Xue, B.; Qin, M.; Cao, Y.; Li, Y.; Wang, W. Printable Fluorescent Hydrogels Based on Self-Assembling Peptides. *Sci. Rep.* **2017**, *7*, 9691.

(22) Li, Y.; Liu, W.; Cheng, L.; Huang, P.; Peng, Y.; Wu, Y.; Li, X.; Li, X.; Fan, X. A Smart pH-Responsive Three Components Luminescent Hydrogel. *J. Funct. Biomater.* **2016**, *7*, 25.

(23) Anasori, B.; Lukatskaya, M. R.; Gogotsi, Y. 2D Metal Carbides and Nitrides (MXenes) for Energy Storage. *Nat. Rev. Mater.* **2017**, *2*, 16098.

(24) Kim, H.; Wang, Z. W.; Alshareef, H. N. MXetronics: Electronic and Photonic Applications of MXenes. *Nano Energy* **2019**, *60*, 179−197.

(25) Naguib, M.; Kurtoglu, M.; Presser, V.; Lu, J.; Niu, J.; Heon, M.; Hultman, L.; Gogotsi, Y.; Barsoum, M. W. Two-Dimensional Nanocrystals Produced by Exfoliation of Ti_3AlC_2. *Adv. Mater.* **2011**, *23*, 4248−4253.

(26) Naguib, M.; Mashtalir, O.; Carle, J.; Presser, V.; Lu, J.; Hultman, L.; Gogotsi, Y.; Barsoum, M. W. Two-Dimensional Transition Metal Carbides. *ACS Nano* **2012**, *6*, 1322−1331.

(27) Ghidiu, M.; Lukatskaya, M. R.; Zhao, M.-Q.; Gogotsi, Y.; Barsoum, M. W. Conductive Two-Dimensional Titanium Carbide 'Clay' with High Volumetric Capacitance. *Nature* **2014**, *516*, 78−81.

(28) Jiang, Q.; Kurra, N.; Maleski, K.; Lei, Y.; Liang, H.; Zhang, Y.; Gogotsi, Y.; Alshareef, H. N. On-Chip MXene Microsupercapacitors for AC-Line Filtering Applications. *Adv. Energy Mater.* **2019**, 1901061.

(29) Boota, M.; Anasori, B.; Voigt, C.; Zhao, M.-Q.; Barsoum, M. W.; Gogotsi, Y. Pseudocapacitive Electrodes Produced by Oxidant-Free Polymerization of Pyrrole between the Layers of 2D Titanium Carbide (MXene). *Adv. Mater.* **2016**, *28*, 1517−1522.

(30) Lei, Y.; Zhao, W.; Zhang, Y.; Jiang, Q.; He, J. H.; Baeumner, A. J.; Wolfbeis, O. S.; Wang, Z. L.; Salama, K. N.; Alshareef, H. N. A MXene-Based Wearable Biosensor System for High-Performance *In Vitro* Perspiration Analysis. *Small* **2019**, *15*, 1901190.
(31) Cai, Y.-C.; Shen, J.; Ge, G.; Zhang, Y.-Z.; Jin, W.-Q.; Huang, W.; Shao, J.-J.; Yang, J.; Dong, X.-C. Stretchable $Ti_3C_2T_x$ MXene/Carbon Nanotubes Composite Based Strain Sensor with Ultrahigh Sensitivity and Tunable Sensing Range. *ACS Nano* **2018**, *12*, 56−62.
(32) Alhabeb, M.; Maleski, K.; Anasori, B.; Lelyukh, P.; Clark, L.; Sin, S.; Gogotsi, Y. Guidelines for Synthesis and Processing of Two-Dimensional Titanium Carbide ($Ti_3C_2T_x$ MXene). *Chem. Mater.* **2017**, *29*, 7633−7644.
(33) Qin, L.; Tao, Q.; Liu, X.; Fahlman, M.; Halim, J.; Persson, P. O.; Rosen, J.; Zhang, F. Polymer-MXene Composite Films Formed by MXene-Facilitated Electrochemical Polymerization for Flexible Solid-State Microsupercapacitors. *Nano Energy* **2019**, *60*, 734−742.
(34) Boota, M.; Anasori, B.; Voigt, C.; Zhao, M. Q.; Barsoum, M. W.; Gogotsi, Y. Pseudocapacitive Electrodes Produced by Oxidant-Free Polymerization of Pyrrole Between the Layers of 2D Titanium Carbide (MXene). *Adv. Mater.* **2016**, *28*, 1517−1522.
(35) Ling, Z.; Ren, C. E.; Zhao, M. Q.; Yang, J.; Giammarco, J. M.; Qiu, J.; Barsoum, M. W.; Gogotsi, Y. Flexible and Conductive MXene Films and Nanocomposites with High Capacitance. *Proc. Natl. Acad. Sci. U. S. A.* **2014**, *111*, 16676−16681.
(36) Chen, C.; Boota, M.; Xie, X.; Zhao, M.; Anasori, B.; Ren, C. E.; Miao, L.; Jiang, J.; Gogotsi, Y. Charge Transfer Induced Polymerization of EDOT Confined-between 2D Titanium Carbide Layers. *J. Mater. Chem. A* **2017**, *5*, 5260−5265.
(37) Zhang, Y.-Z.; Lee, K. H.; Anjum, D. H.; Sougrat, R.; Jiang, Q.; Kim, H.; Alshareef, H. N. MXenes Stretch Hydrogel Sensor Performance to New Limits. *Sci. Adv.* **2018**, *4*, No. eaat0098.
(38) Debye, P. A. Method for the Determination of the Mass of Electrolyte Ions. *J. Chem. Phys.* **1933**, *1*, 13−16.
(39) Rutgers, A. J.; Rigole, W. Ultrasonic Vibration Potentials in Colloid Solutions, in Solutions of Electrolytes and Pure Liquids. *Trans. Faraday Soc.* **1958**, *54*, 139−143.
(40) Dukhin, S. S.; Mischuk, N. A.; Kuz'menko, B. B.; Il'in, B. I. Streaming Current and Potential-in a High-Frequency Acoustic Field. *Colloid J.* **1983**, *45*, 875−881.
(41) Dukhin, A. S. Observation of Sol-Gel Transition for Carbon Nanotubes Using Electroacoustics: Colloid Vibration Current *versus* Streaming Vibration Current. *J. Colloid Interface Sci.* **2007**, *310*, 270−280.
(42) Bushberg, J. T.; Seibert, J. A.; Leidholdt, E. M.; Boone, J. M. *The Essential Physics of Medical Imaging*; Lippincott Williams & Wilkins: Philadelphia, 2002; pp 469−553.
(43) Shankar, H.; Pagel, P. S. Potential Adverse Ultrasound-Related Biological Effects: A Critical Review. *Anesthesiology* **2011**, *115*, 1109−1124.
(44) Chen, A. I.; Balter, M. L.; Chen, M. I.; Gross, D.; Alam, S. K.; Maguire, T. J.; Yarmush, M. L. Multilayered Tissue Mimicking Skin and Vessel Phantoms with Tunable Mechanical, Optical, and Acoustic Properties. *Med. Phys.* **2016**, *43*, 3117−3131.
(45) Lyklema, J. *Fundamental of Interface and Colloid Science*. Solid-Liquid Interfaces; Academic Press: London, 1995; Vol. 2, pp 779.
(46) van der Heyden, F. H.; Bonthuis, D. J.; Stein, D.; Meyer, C.; Dekker, C. Power Generation by Pressure-Driven Transport of Ions in Nanofluidic Channels. *Nano Lett.* **2007**, *7*, 1022−1025.
(47) Yang, J.; Lu, F.; Kostiuk, L. W.; Kwok, D. Y. Electrokinetic Microchannel Battery by Means of Electrokinetic and Microfluidic Phenomena. *J. Micromech. Microeng.* **2003**, *13*, 963.
(48) Stanley, J. S. The Effect of Paraffin Chain Salts on the Charge on Textile Fibers. *J. Phys. Chem.* **1954**, *58*, 533−536.
(49) Jacobasch, H.-J.; Bauböck, G.; Schurz, J. Problems and Results of Zeta-Potential Measurements on Fibers. *Colloid Polym. Sci.* **1985**, *263*, 3.
(50) Xie, H.; Saito, T.; Hickner, M. A. Zeta Potential of Ion-Conductive Membranes by Streaming Current Measurements. *Langmuir* **2011**, *27*, 4721−4727.
(51) Kim, K. J.; Fane, A. G.; Nystrom, M.; Pihlajamaki, A. Chemical and Electrical Characterization of Virgin and Protein-Fouled Polycarbonate Track-Etched Membranes by FTIR and Streaming-Potential Measurements. *J. Membr. Sci.* **1997**, *134*, 199.
(52) Shahid U N, M.; Deshpande, A. P; Rao, C L. Electro-Mechanical Properties of Hydrogel Composites with Micro-and Nano-Cellulose Fillers. *Smart Mater. Struct.* **2015**, *24*, 095013.
(53) Fiumefreddo, A.; Utz, M. Bulk Streaming Potential in Poly (Acrylic Acid)/Poly (Acrylamide) Hydrogels. *Macromolecules* **2010**, *43*, 5814−5819.
(54) Zhan, C.; Naguib, M.; Lukatskaya, M.; Kent, P. R.; Gogotsi, Y.; Jiang, D. E. Understanding the MXene Pseudocapacitance. *J. Phys. Chem. Lett.* **2018**, *9*, 1223−1228.
(55) Niu, S.; Wang, S.; Lin, L.; Liu, Y.; Zhou, Y. S.; Hu, Y.; Wang, Z. L. Theoretical Study of Contact-Mode Triboelectric Nanogenerators as an Effective Power Source. *Energy Environ. Sci.* **2013**, *6*, 3576−3583.
(56) Diaz, A. F.; Felix-Navarro, R. M. A Semi-Quantitative Tribo-Electric Series for Polymeric Materials: The Influence of Chemical Structure and Properties. *J. Electrost.* **2004**, *62*, 277−290.
(57) Cafarelli, A.; Miloro, P.; Verbeni, A.; Carbone, M.; Menciassi, A. Speed of Sound in Rubber-based Materials for Ultrasonic Phantoms. *J. Ultrasound* **2016**, *19*, 251−256.
(58) Ludwig, G. D. The Velocity of Sound through Tissues and the Acoustic Impedance of Tissues. *J. Acoust. Soc. Am.* **1950**, *22*, 862−866.

https://dx.doi.org/10.1021/acsnano.9b08462
ACS Nano 2020, 14, 3199−3207